Journal of Materials Chemistry C

PAPER

View Article Online
View Journal | View Issue

Cite this: J. Mater. Chem. C, 2015, 3, 4269

Development of tilt, biaxiality and polar order in bent-core liquid crystals derived from 4′-hydroxybiphenyl-3-carboxylic acid†

Dilek Güzeller,[a] Hale Ocak,*[ab] Belkız Bilgin-Eran,[a] Marko Prehm[bc] and Carsten Tschierske*[b]

Received 5th January 2015,
Accepted 16th March 2015

DOI: 10.1039/c5tc00015g

www.rsc.org/MaterialsC

A homologous series of unsymmetric bent-core compounds derived from 4′-hydroxybiphenyl-3-carboxylic acid and having strongly distinct chains at both ends has been synthesized and characterized. The liquid crystalline self-assembly of the compounds was investigated by differential scanning calorimetry, optical polarizing microscopy, X-ray scattering and electro-optic methods. With increasing chain length and upon cooling a series of smectic phases was observed, starting from SmA phases having an unusual structure composed of domains with a randomized tilt direction. This is followed by a series of biaxial smectic phases, involving a smectic phase composed of tilt domains with increased size (SmC_r), anticlinic and synclinic tilted smectic phases (SmC_s, SmC_a) and finally columnar phases with an oblique (Col_{obl}) or pseudo-rectangular (Col_{rec}) lattice. This phase sequence is the result of the competition between an emerging tilt, the dense packing of the bent aromatic cores leading to restricted rotation and contributing to phase biaxiality, and the steric distortion of the dense packing by the bulky 3,7-dimethyloctyloxy chains, inhibiting the formation of long range polar order. In all smectic phases the tilt is relatively small, thus providing only weak layer coupling and this provides the basis for sensitive regulatory networks determining the mode of molecular self-assembly in the resulting LC phases. The columnar phases have a tilted B_{1rev}-like ribbon structure with a temperature and chain length dependent inversion of the sign of birefringence. Though none of the racemic compounds show polar switching, the (*S*)-enantiomer of one compound shows ferroelectric-like switching in an anticlinic tilted smectic phase (SmC_aP_R*).

1. Introduction

Bent-core liquid crystals represent one of the most exciting subclasses of the thermotropic liquid crystals (LC) due to their remarkable and unique properties, such as macroscopic polar order and spontaneous mirror symmetry breaking, which are of significant interest for fundamental soft matter science as well as for potential applications in ferroelectric and NLO active materials.[1–8] Further applications involve the use of the dense packing of the π-conjugated aromatic cores in some of the LC phases for semiconducting materials and the application in alignment layers.[9,10] Moreover, the spontaneous symmetry breaking in several LC phases of bent-core molecules provides a source of superstructural chirality for chiral separation and chiral induction.

Initially, resorcinol bisbenzoates involving additional imine units between the benzene rings of the bent aromatic core were used as building blocks.[11] Some years later it was found that COO groups,[12] and later the C=C groups[13] and N=N groups,[14] also can replace the labile imines, providing new opportunities in mesophase diversity and applicability. Thus, numerous "banana phases" (B_1–B_8) were discovered,[1,2,4] among them were tilted, non-tilted and "double tilted" (Sm_G)[15,16] flat, undulated and modulated lamellar (smectic) phases with macroscopic or local polar order.[2,17] In some cases transitions between polar mesophases of bent-core mesogens and the well-known mesophases of rod-like LCs, such as nematic, SmA and SmC phases were also observed and unusual properties were identified for most of these LC phases.[4,18–21] Examples are cybotactic nematic phases (N_{cyb})[22–24] and biaxial SmA phases (SmA_b).[25–32]

[a] Department of Chemistry, Yildiz Technical University, Davutpasa Yerlesim Birimi, TR-34220, Esenler, Istanbul, Turkey. E-mail: ocak_hale@hotmail.com
[b] Institute of Chemistry, Organic Chemistry, Martin Luther University Halle-Wittenberg, Kurt-Mothes-Str. 2, D-06120 Halle, Germany. E-mail: Carsten.tschierske@chemie.uni-halle.de
[c] Institute of Chemistry, Physical Chemistry, Martin Luther University Halle-Wittenberg, Von-Danckelmann-Platz 4, D-06120 Halle, Germany

† Electronic supplementary information (ESI) available. See DOI: 10.1039/c5tc00015g

Most bent-core mesogens form strongly tilted SmC phases with tilt angles in the range of 35–45°. This strong tilt is of relevance in the development of chirality, but it is disadvantageous for their application in electro-optical devices. In recent years, bent-core compounds showing various weakly tilted and non-tilted smectic phases, namely uniaxial SmA phases with local polar order ($SmAP_R$),[33–35] non-polar but biaxial SmA_b phases[32,36] as well as polar $SmAP_A$[37] and $SmAP_F$ phases,[38] attracted significant interest.[37,39–42] These non-tilted smectic phases provide access to the application of bent-core molecules in electro-optical display devices having one to two orders of magnitude faster switching modes[43] than the presently used displays based on nematic mixtures;[44] especially short switching-off times were realized.[45] Therefore, the search for new materials showing non-tilted or weakly tilted biaxial smectic phases is of significant importance for improving material properties and for new applications. Most compounds forming non-tilted smectic phases involve terephthalate units in the rod-like wings,[46] or have bent units representing esters of 3-hydroxybenzoic acid,[25–27,41] 4′-hydroxybiphenyl-3-carboxylic acid[16,35,42,47] or 3′-hydroxybiphenyl-4-carboxylic acid,[16,38,48] In contrast, bent-core mesogens with rod-like wings derived from 4-hydroxybenzoic acid and those having bent units representing esters of resorcinol[1,2] or 3,4′-biphenyldiol[12] with a reversed orientation of some COO groups, show highly tilted SmC phases. Thus, the orientation of the linking group connecting the aromatic rings of the bent-core plays an important role in the mode of LC self assembly[49–52] as it influences polarity, electron density distribution and bending angle which strongly affect the type of the formed mesophase.[53]

The aim of this study is to gain a better understanding of the distinct molecular structural effects on the development of polar order, phase biaxiality, tilt and layer undulations in smectic phases of bent-core mesogens to develop design rules for materials forming a predominately non-tilted and weakly tilted polar smectic phase. To this end a new series of bent-core compounds with highly unsymmetrical structure was synthesized. These compounds involve a bent unit derived from 4′-hydroxybiphenyl-3-carboxylic acid. Only one linear alkoxy group or an olefin-terminated alkoxy chain was attached to one end of the bent-core and a much bulkier branched and inherently chiral 3,7-dimethyloctyloxy group (see Fig. 1) was attached to the other end. Besides the effect of the 4′-hydroxybiphenyl-3-carboxylate core structure and chain branching, focus is also on the influence of molecular chirality on LC self assembly in this class of compounds. For this purpose two representative examples were prepared as enantiomers with (*S*)-configuration of the 3,7-dimethyloctyloxy chain.[54] In the compound names (*rac*-***n*** and (*S*)-***n***) the number of carbons in the non-branched chain is indicated by ***n*** and the configuration of the chiral carbon in the 3,7-dimethyloctyloxy chain is added as prefix, where *rac* is used for the racemic mixtures. These new compounds were analyzed by polarizing microscopy, DSC, XRD and electro-optical methods to obtain information on their self-assembly in LC phases. It is shown that with the growing chain length and decreasing temperature a series of smectic phases is observed, starting with SmA phases having an unusual structure composed of synclinic SmC domains with a randomized tilt direction. It is followed by biaxial smectic phases, among them a SmC phase with an enlarged size of these tilt-domains (SmC_r) and weakly anticlinic (SmC_a) or synclinic tilted (SmC_s) smectic phase with appreciable molecular biaxiality, and finally by columnar phases with oblique (Col_{obl}) or pseudo-rectangular (Col_{rec}) lattices. This phase sequence is discussed as the result of a competition between a relatively small tilt providing only weak layer coupling, a restriction of the rotation around the long axis due to the dense packing of the bent aromatic cores, and the steric distortion of the dense packing by the bulky 3,7-dimethyloctyloxy chains. Though none of the racemic compounds show polar switching, the anticlinic SmC_aP_R* phase of the (*S*)-enantiomer of one compound exhibits ferroelectric-like switching.

2. Results and discussion

2.1 Synthesis

The bent-core compounds *rac*-***n*** and (*S*)-***n*** were synthesized as shown in Scheme 1. The 4′-benzyloxybiphenyl-3-carboxylic acid **A**[18,47] was synthesized by Pd(0)-catalyzed Suzuki cross-coupling reaction[55] of commercially available methyl 3-bromobenzoate with 4-benzyloxyphenylboronic acid,[56] followed by saponification of the thus obtained methyl ester.

For the synthesis of the 4-hydroxybenzoate (*S*)-**B**, (*S*)-(−)-β-citronellol was at first hydrogenated (H_2, Pd/C in MeOH, 5 bar) to give (*S*)-3,7-dimethyl-1-octanol which was then converted to (*S*)-3,7-dimethyloctyl-1-bromide (conc. aqu. HBr, conc. H_2SO_4).[57] Etherification with 4-benzyloxyphenol, followed by hydrogenolytic debenzylation (H_2, Pd in 5 bar) provided (*S*)-4-(3,7-dimethyloctyloxy)phenol.[58] The esterification of (*S*)-4-(3,7-dimethyloctyloxy)phenol with

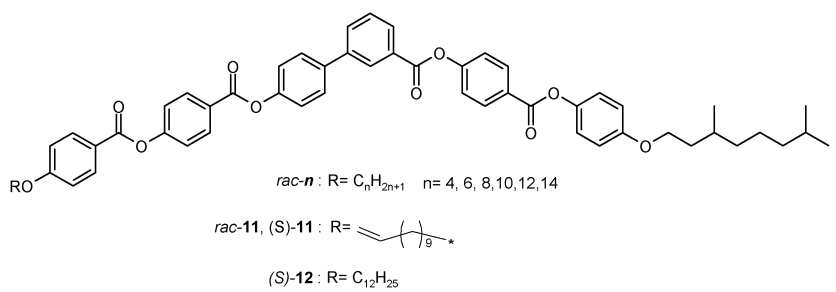

Fig. 1 Bent-core compounds under investigation.

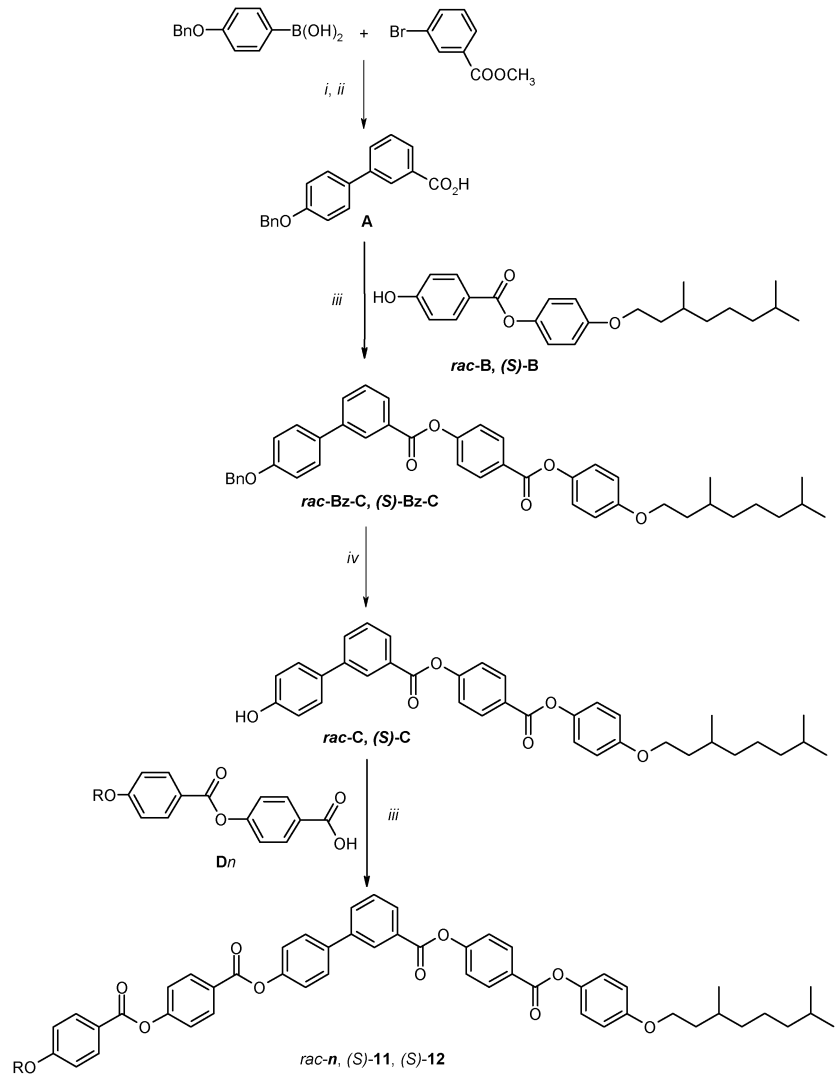

Scheme 1 Synthesis of the bent-core compounds *rac*-***n*** and (*S*)-***n*** (for ***n***, see Fig. 1). *Reagents and conditions*: (i) cat. $[Pd(PPh_3)_4]$, $NaHCO_3$, H_2O, glyme, reflux 4 h;[55] (ii) KOH, EtOH, reflux 2 h; (iii) DCC, DMAP, CH_2Cl_2, r.t.;[65] (iv) H_2, Pd/C, THF, 40 °C, 18 h.[56]

4-benzyloxybenzoic acid[59] and subsequent hydrogenolytic debenzylation (H_2, 10% Pd/C in THF, 5 bar) yielded (*S*)-**B**. The racemic compound *rac*-**B** was prepared in a similar way from racemic 3,7-dimethyl-1-octanol *via* the tosylate as described previously.[60,61] Esterification of the thus obtained 4-hydroxybenzoates *rac*-**B** and (*S*)-**B** with 4′-benzyloxybiphenyl-3-carboxylic acid **A**[18,47] followed by hydrogenolytic debenzylation[56] gave the biphenylols *rac*-**C** and (*S*)-**C**. From these biphenylols the bent-core compounds *rac*-***n*** and (*S*)-***n*** were obtained by acylation with the appropriate benzoic acids **D*n***.[12,62–64] DCC/DMAP was used for all acylation reactions.[65] The 4-(4-*n*-alkyloxybenzoyloxy)benzoic acids **D4–D14** and 4-[4-(10-undecenyloxy)-benzoyloxy]benzoic acid **D11**[66,67] were obtained by the esterification of appropriate 4-substituted benzoic acids with 4-hydroxybenzaldehyde, followed by oxidation using sodium chlorite as the oxidizing agent.[68] The experimental details, spectroscopic (^{1}H-, ^{13}C-NMR and MS) and analytical data of the intermediates and final compounds are given in the ESI.†

Throughout all steps of the synthesis of the enantiomers (*S*)-**11** and (*S*)-**12** the stereogenic center of the (*S*)-3,7-dimethyloctyloxy group was not touched, and hence, it can be assumed that the final products have approximately equal enantiomeric purity as (*S*)-(−)-β-citronellol (>95%) used as starting material.[20,69,70]

2.2 Optical investigations and DSC

The observed transition temperatures, corresponding enthalpy values and mesophase types are summarized in Table 1. All compounds form enantiotropic (thermodynamically stable) LC phases with LC-Iso transition temperatures in the range between 155 and 163 °C and melting points around 103–139 °C. Also the odd-numbered compounds *rac*-**11** and (*S*)-**11** incorporating an additional double bond at the end of the alkyl chain fit into this series. The shortest homologue *rac*-**4** has only a uniaxial smectic phase (SmA). On increasing the number of carbon atoms in the linear alkoxy chain the SmA phase region becomes smaller

Table 1 Mesophases, phase transition temperatures as observed on heating (H →) and cooling (← C) and corresponding transition enthalpies of the compounds *rac*-**4**–*rac*-**14**, (*S*)-**11** and (*S*)-**12**[a]

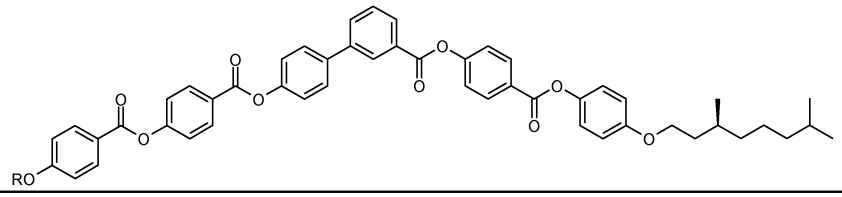

Comp.	R	T/°C [ΔH kJ mol^{-1}]
rac-**4**	—C_4H_9	H →: Cr_1 120 [7.9] Cr_2 130 [21.9] SmA 160 [2.1] Iso Cr 123 [17.1] SmA 155 [2.2] Iso: ← C
rac-**6**	—C_6H_{13}	H →: Cr 139 [30.4] Col_{obl} 146 [3.3] SmA 155 [3.5] Iso Cr 132 [28.1] Col_{obl} 145 [3.5] SmA 153 [3.5] Iso: ← C
rac-**8**	—C_8H_{17}	H →: Cr 133 [24.5] Col_{obl} 151 [4.6] SmC 156 [<0.1] SmA 159 [4.7] Iso Cr 125 [25.5] Col_{obl} 150 [4.3] SmC 155 [<0.1] SmA 158 [4.7] Iso: ← C
rac-**10**	—$C_{10}H_{21}$	H →: Cr 110 [14.6] Col_{rec} 133 [2.5] SmC_s 145 [<0.1] SmC_a 152 SmC_r 153 SmA 155 [4.4][b] Iso Cr 103 [13.1] Col_{rec} 130 [2.1] SmC_s 145 [<0.1] SmC_a 151 SmC_r 152 SmA 154 [4.3][b] Iso: ← C
rac-**11**	—$(CH_2)_9CH{=}CH_2$	H →: Cr 111 [15.6] Col_{rec} 139 [1.1] SmC_s147 [0.03] SmC_a 160 [6.2] Iso Cr 106 [14.7] Col_{rec} 137 [1.2] SmC_s 144 [0.04] SmC_a 158 [5.6] Iso: ← C
(*S*)-**11**	—$(CH_2)_9CH{=}CH_2$	H →: Cr 111 [18.3] Col_{rec} 140 [2.1] SmC_s*147 [0.04] SmC_a*160 [6.2] Iso Cr 106 [16.6] Col_{rec} 138 [2.2] SmC_s*144 [0.04] SmC_a*158 [6.1] Iso: ← C
rac-**12**	—$C_{12}H_{25}$	H →: Cr 103 [17.7] Col 137 [1.3] SmC_s 145 [<0.1] SmC_a161 [5.9] Iso Cr 99 [9.1] Col 135 [1.0] SmC_s 143 [<0.1] SmC_a 160 [5.9] Iso: ← C
(*S*)-**12**	—$C_{12}H_{25}$	H →: Cr 103 [39.3] Col 134 [1.3] SmC_s* 142 [<0.1] SmC_aP_R* 158 [5.9] Iso Cr 99 [9.3] Col 133 [1.6] SmC_s*138 [<0.1] SmC_aP_R* 157 [5.3] Iso: ← C
rac-**14**	—$C_{14}H_{29}$	H →: Cr 105 [22.9] Col_{obl} 138 [1.0] SmC_s 145 [<0.1] SmC_a 163 [7.3] Iso Cr 100 [17.8] Col_{obl} 135 [1.2] SmC_s 143 [<0.1] SmC_a 162 [6.5] Iso: ← C

[a] Abbreviations: Cr = crystalline solid state; Iso = isotropic liquid; SmA = non-tilted smectic LC phase; SmC = synclinic tilted smectic phase with nearly complete rotational disorder around the molecular long axis; SmC_s = SmC phase with synclinic tilted organization of the molecules and restricted rotation around the molecular long axis; Sm_a = SmC_s phase with weak layer coupling and combining synclinic and anticlinic layer correlation; SmC_r = smectic phase composed of medium sized SmC_s domains with randomized tilt direction; Col = columnar LC phase; Col_{obl} = columnar LC phase with oblique lattice; (corresponding to SmC = synclinic tilted SmC phase with long range layer modulation on an oblique lattice); Col_{rec} = Col_{obl} phase with pseudo-rectangular columnar lattice (γ in the oblique lattice is ~90°); * indicates chiral versions of these phases formed by the (*S*)-enantiomers; SmC_aP_R* = chiral SmC_a phase showing a relatively broad single polarization peak indicative of switching of field-induced ferroelectric domains. [b] Enthalpy value involves all three transitions SmC_a–SmC_r–SmA–Iso, individual transition temperatures were determined by PM.

and is gradually replaced by a series of biaxial smectic (SmC, SmC_r, SmC_a, SmC_s) and columnar phases (Col_{obl}/Col_{rec}).

The high temperature smectic phases of compounds *rac*-**4** to *rac*-**10** display fan-shaped textures in *planar alignment* (layers are perpendicular to the substrate surfaces; see Fig. 2a, 3a and 4a for *rac*-**6**, *rac*-**8** and *rac*-**10**, respectively). These textures are typical for non-tilted smectic phases without in-plane order (SmA phases). Another typical feature of these uniaxial smectic phases is that the *homeotropically aligned* samples (layers are parallel to the substrate surfaces) do not appear completely dark between crossed polarizers, as shown in Fig. 2b and 3b for compounds *rac*-**6** and *rac*-**8** as examples. Because rotating the sample between the crossed polarizers does not modify the brightness, there is no optical anisotropy and brightness cannot be due to birefringence. Thus, it is most likely the result of light scattering in these homeotropically aligned uniaxial smectic phases. This would mean that these SmA phases should be composed of domains with a size in the sub-micrometer range. As the LC phases occurring below SmA are tilted (see below) the most likely possibility would be a micro-domain structure composed of uniformly tilted micro-domains with degenerated azimuthal distribution. Thus, these SmA phases could possibly be regarded as a special kind of ''de Vries like'' SmA phases[71] composed of uniformly tilted domains with appreciable size. The small tilt and the denser packing of the bent-core aromatics in a tilted arrangement might be considered as the driving forces for the formation of this unusual phase structure.

For compound *rac*-**6** the SmA phase is accompanied by a columnar phase at temperatures below T = 145 °C, as indicated by the transition to a mosaic-like appearance of the fan-like texture in planar samples (Fig. 2c) and by the formation of a low birefringent spherulitic texture occurring in homeotropically aligned samples (Fig. 2d). XRD investigations (see Section 2.4) indicate an oblique lattice (Col_{obl}), which is assumed to result from a tilted organization of the molecules in ribbons.

For compound *rac*-**8** the SmA phase (Fig. 3a and b) and the columnar phase (Fig. 3e and f) are separated by an additional optically biaxial smectic phase as indicated by the occurrence of a typical birefringent schlieren texture in homeotropic aligned samples (Fig. 3c and d). In some areas domains with alternating tilt direction can be distinguished (Fig. 3d).[72] The investigation of samples in planar alignment indicates the onset of a tilt of about 10° at the uniaxial-biaxial transition and the occurrence of a broken fan texture as typical for synclinic SmC phases (Fig. 3a, c and e). The increase of birefringence at the SmA–SmC transition, as indicated by a color change of the fans from blue to green, supports the proposed de Vries-like

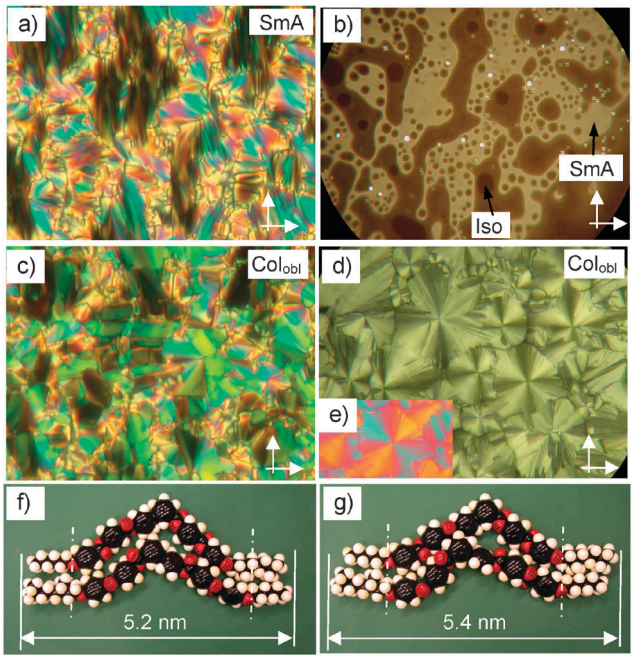

Fig. 2 (a–e) Textures of the LC phases of compound *rac*-**6** as observed between crossed polarizers (indicated by arrows), (a, c) in a 6 μm PI-coated ITO cell providing planar alignment and (b, d, e) between non-treated glass slides with homeotropic alignment: (a) SmA phase at T = 150 °C; (b) SmA–Iso transition at T = 155 °C (bright areas = SmA, dark areas = Iso, intermediate gray levels result from areas where SmA surface layers coexist with the isotropic bulk); (c, d) Col$_{obl}$ phase at T = 141 °C; (e) shows the homeotropic texture with an additional λ-retarder plate, indicating positive birefringence (blue shifted fans in southeast-northwest orientation and yellow shifted fans in the other direction). (f, g) show CPK models of *rac*-**6** for different antiparallel packing modes (f) with optimized core packing and some mixing of aromatic cores and alkyl chains, and (g) with maximized core-chain segregation and optimized alkyl chain packing, but distorted core packing.

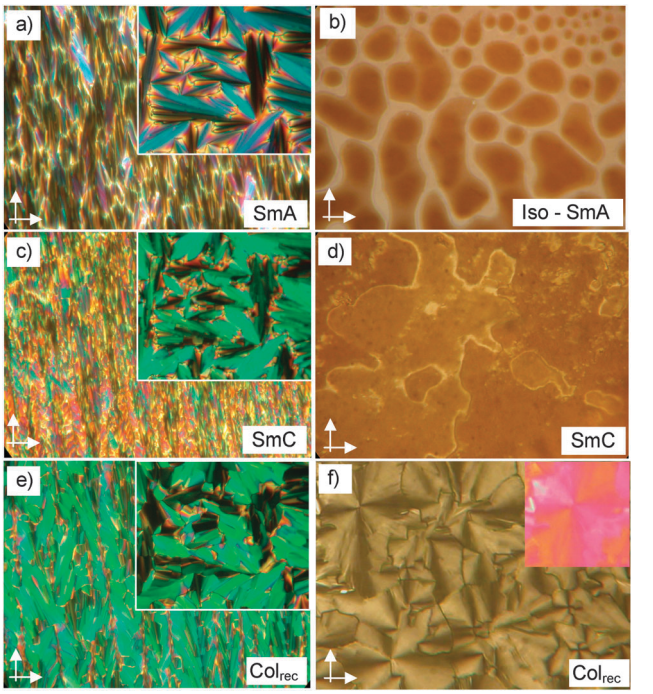

Fig. 3 Textures of the LC phases of compound *rac*-**8** as observed between crossed polarizers (indicated by arrows) in (a, c, e) with planar alignment in a 6 μm PI-coated ITO cell (rubbing direction is horizontal, the insets show the corresponding fan-like textures) and (b, d, f) between non-treated microscopic slides, showing predominately homeotropic alignment: (a) SmA phase at T = 157 °C; (b) SmA–Iso transition at T = 159 °C, (c, d) SmC phase at T = 152 °C, and (e, f) Col$_{obl}$ phase at T = 140 °C, the inset shows the texture with an additional λ-retarder plate indicating positive birefringence.

tilt-domain structure of the SmA phase.[71c] The columnar phase occurring below this SmC phase has textural features very similar to that observed for the Col$_{obl}$ phase of compound *rac*-**6** (Fig. 3e and f). The major enthalpy change is found for the SmC–Col$_{obl}$ transition (4.3 kJ mol^{-1}), whereas the transition enthalpy SmA–SmC is not visible in the DSC traces (<0.1 kJ mol^{-1}, see Table 1 and Fig. S12, ESI†).

The next even numbered homologue *rac*-**10** has totally five different LC phases. In all LC phases the wide angle scattering is diffuse, confirming true LC phases without in-plane order (see Section 2.3). On cooling the planar aligned samples of the SmA phase a transition is observed at T = 152 °C, (Fig. 4a and b and Fig. S1f, ESI†). At this phase transition the dark extinctions in the planar SmA texture mostly become birefringent which indicates a tilted organization of the molecules in this phase, designated herein as SmC$_r$ (see below). In homeotropic alignment a weakly birefringent schlieren texture appears at the SmA–SmC$_r$ transition which increases in brightness with decreasing temperature (Fig. 4e). Remarkably, the overall brightness does not significantly change by rotation of the sample between crossed polarizers (similar to the weak birefringence in the homeotropic SmA phase) and hence, also in this phase there seems to be a significant contribution of light scattering to the overall brightness of the homeotropic samples. Thus, it seems that at the SmA–SmC$_r$ transition the synclinic tilted micro domains reach a size which exceeds the wavelength of light. There is only a short coherence length of the tilt direction in the bulk (therefore the assignment as SmC$_r$, where subscript "r" indicates a kind of "randomized" tilt), but macroscopic alignment – leading to a macrosopic SmC$_s$ structure – is easily obtained at surfaces. Especially in planar cells large uniformly synclinic tilted domains can develop due to surface pinning, giving rise to the texture shown in Fig. 4b.[73] This phase is stable only over a very small temperature range of about 1 K and upon further cooling to 151 °C the dark extinctions reappear at the same positions with an orientation parallel to the polarizer as in the SmA phase above (Fig. 4c).

In planar samples with fan texture (see insets in Fig. 4a–c) the birefringence increases at the SmA–SmC$_r$ transition and then decreases again at the transition from SmC$_r$ to the next LC phase (SmC$_a$). The only difference between the fans in the SmA phase and in this phase is the formation of fine purple stripes occurring across the blue fans, which can be recognized by a careful inspection of the inset in Fig. 4c. The brightness of the homeotropic texture decreases at this transition, light scattering disappears and the distinct direction of the secondary optical axis can be distinguished by rotating the sample

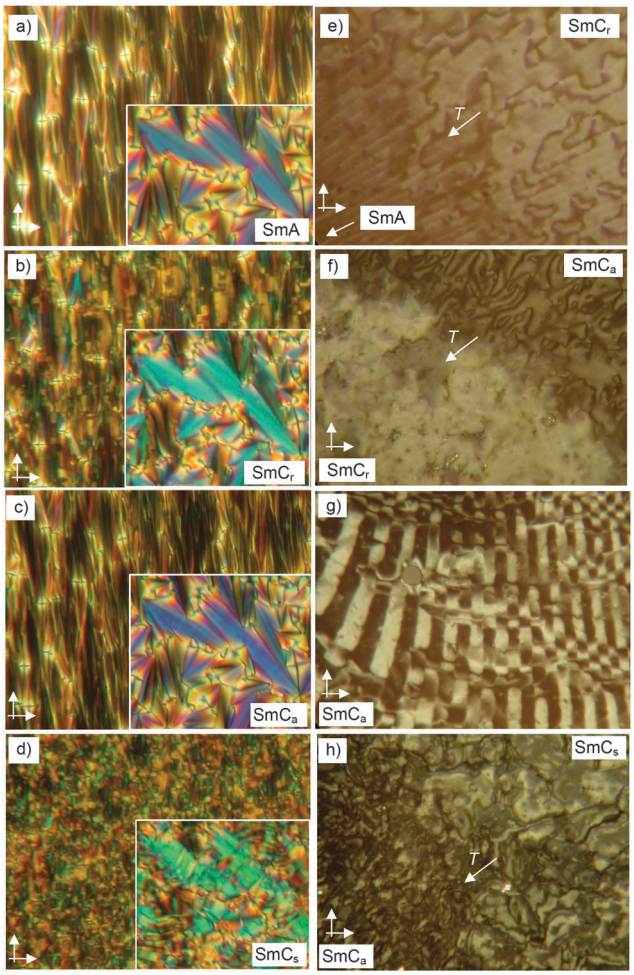

Fig. 4 Textures of the LC phases of compound *rac*-**10** as observed between crossed polarizers (horizontal and vertical): (a–d) samples with planar alignment in a 6 μm ITO cell (rubbing direction is horizontal, the insets show the corresponding fan-like textures) and (e–h) between non-treated microscopic slides with homeotropic alignment, (e, f) and (h) with temperature gradient as indicated by arrows (direction of the development of the texture on cooling; arrow from lower to higher *T*); (a) SmA phase at T = 153 °C; (b) SmC$_r$ phase at T = 152 °C; (c) SmC$_a$ phase at T = 151 °C; (d) SmC$_s$ phase at T = 136 °C; (e) typical stripes occurring at the SmA–SmC$_r$ transition at T = 153 °C; (f) SmC$_r$–SmC$_a$-transition at T = 152 °C; (g) stripe texture in the SmC$_a$ phase at T = 148 °C and (h) Sm$_a$–SmC$_s$ transition at T = 145 °C (for additional textures, see Fig. S1, ESI†).

between crossed polarizers (Fig. 4f and Fig. S1e, ESI†). These optical observations could mean that at this transition either the tilt is removed, which could indicate a transition to a biaxial SmA phase (SmA$_b$), or that the tilt becomes anticlinic, leading to an anticlinc tilted SmC$_a$ phase. The remarkable feature of the SmC$_r$ phase is the appearance of a regular periodic stripe pattern in homeotropic samples at the SmA–SmC$_r$ transition, as observed on slow cooling (1 K min^{-1}) and shown in Fig. 4e. This stripe pattern, once formed, is retained also in the SmC$_a$ phase and there it can occur with impressive regularity and contrast (Fig. 4g and Fig. S1a and b, ESI†). Such patterns have previously been observed for homeotropic aligned biaxial SmA phases (SmA$_b$ phases)[32,74] and have sometimes been considered as a typical feature of these phases.[47,74,75] However, there are also reports on anticlinic tilted SmC$_a$ phases showing similar stripe patterns,[47,76,77] so that this feature appears to be not directly related to the SmA$_b$ structure.[78] Though we have no clear explanation for the occurrence of this stripe pattern, it is due to an alternation of the secondary optical axis in the biaxial smectic phases (see Fig. S1b, ESI†) and could probably be associated with the development of phase biaxiality of lamellar LC phases from a phase with a local biaxial domain structure. As the layer spacing decreases in the temperature range of the biaxial smectic phases (see Section 2.3), the formation of an anticlinic tilted SmC$_a$ phase is likely.

On further cooling the transition to a synclinic SmC phase (SmC$_s$, Fig. 4d) and then to a columnar phase (Fig. S1d, ESI†) takes place. As shown in the circular domains in Fig. 5 the tilt is ~12° in the SmC$_s$ phase and increases to $\beta \sim 16°$ in the Col$_{rec}$ phase of *rac*-**11**. In the transition to the synclinic SmC$_s$ phase the stripe pattern in the homeotropic textures is erased and the birefringence increases significantly (see Fig. 4h top right and Fig. S1a and c, ESI†). The planar texture of the SmC$_s$ phase is distinct from the usually observed broken fan textures where stripes develop parallel to the fans, as observed for the SmC phase of *rac*-**8** (see insets in Fig. 3a and c). For compounds *rac*-***n***, with n = 10–14 stripe formation takes place perpendicular to the fan direction and a mosaic-like "fan-texture" is formed in planar samples (Fig. 4d). It is postulated that this SmC$_s$ phase is distinct from usual synclinic SmC phases of rod-like molecules (and the SmC phase formed by *rac*-**8**) by a significant restriction of the rotation around the molecular long axis, leading to an additional contribution of molecular biaxiality to the overall

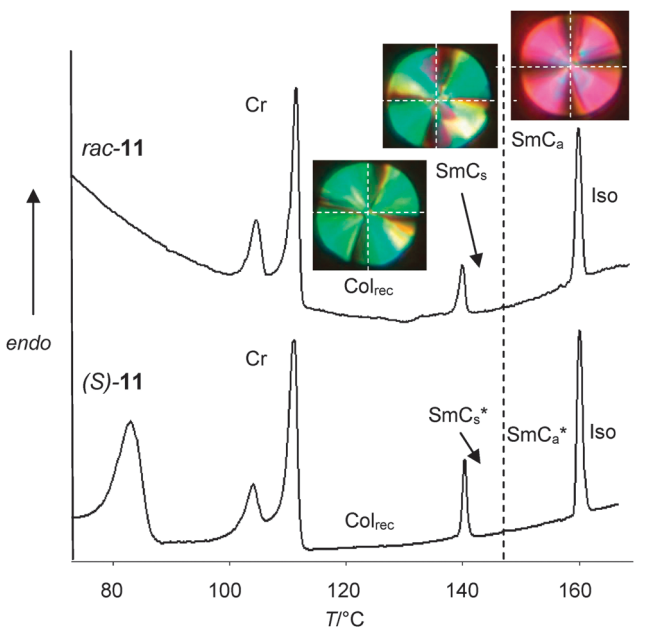

Fig. 5 DSC heating traces (first heating, 10 K min^{-1}) of compounds *rac*-**11** (top) and (*S*)-**11** (bottom); for expanded region of the SmC$_s$–SmC$_a$ transition see Fig. S13 (ESI†). In addition circular domains grown from small droplets of *rac*-**11** are shown, indicating the onset of a small tilt in the SmC$_s$ phase ($\beta \sim 12°$) which increases to $\beta \sim 17°$ in the Col$_{rec}$ phase.

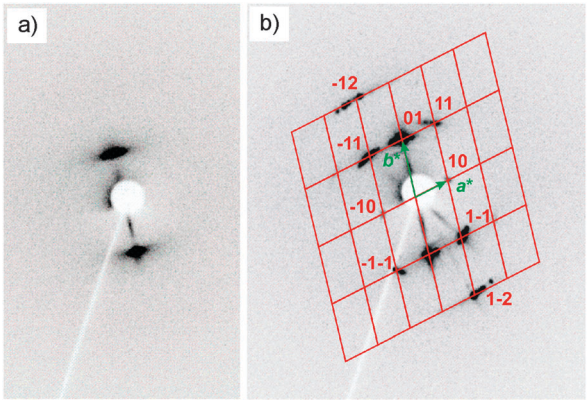

Fig. 6 XRD patterns of compound *rac*-**6** (a) in the SmA at T = 150 °C and (b) in the Col_{obl} phase at T = 140 °C.

phase biaxiality. Though there is restriction of the molecular rotation around the long axis, there seems to be no sufficient coherence of polar coupling between the bent molecules, so that the SmC_s phases are apolar (see Section 2.6).

The transition enthalpy value of the SmC_a–SmC_s transition is below 0.1 kJ mol^{-1} for all compounds (see Fig. 5 and Fig. S13, ESI,† and Table 1), which is in line with an apolar structure of the SmC_s phase. In contrast, there is a significant transition enthalpy for the SmC_s–Col transition which decreases from 2.5 to about 1.0 kJ mol^{-1} with growing alkyl chain length from decyl in *rac*-**10** to tetradecyl in *rac*-**14**. In homeotropic samples there is no visible change in the birefringence at this transition, confirming that the tilt remains synclinic at the SmC_s–Col_{rec} transition (Fig. S1c and d, ESI†). Thus, the 2D periodicity results from the modulation of the SmC_s layers, allowing a denser packing of the bent aromatic cores.[79]

In *rac*-**11**, the SmA and SmC_r phases are removed completely and a SmC_a–SmC_s–Col trimorphism is observed, *i.e.* the SmC_a phase is directly formed at the transition from the isotropic liquid. The DSC heating traces of compounds *rac*-**11** and (*S*)-**11** are shown as representative examples for these compounds in Fig. 5. The formation of the SmC_a phase is indicated in planar aligned samples by stripes with slightly reduced birefringence occurring across the fans; these stripes become more pronounced with the growing alkyl chain length (compare Fig. 4c and Fig. S2a and S3a, ESI†). In contrast, for homeotropic samples of the SmC_a phase the typical dark-bright stripe texture is only observed for compounds *rac*-**10** to *rac*-**12**, but not for compound *rac*-**14** with the longest alkyl chain (Fig. S3d, ESI†). In all cases these stripes disappear and are replaced by more birefringent schlieren textures at the transition to the SmC_s phases. (see Fig. S2a–d and S3d and e, ESI†).[80] More information about the distinct phases was derived from XRD and electro-optical investigations which are described in the following Sections.

2.3 XRD investigation of the smectic phases

The XRD pattern of compound *rac*-**6** in the SmA phase is characterized by a diffuse wide angle scattering and a sharp layer reflection without higher harmonics in the small angle region. The position of the layer reflection corresponds to a layer distance d = 5.1 nm (Fig. 6a), which is almost the same as the molecular length L_{mol} = 5.2 nm, measured in a Λ-shaped conformation with 120° bent aromatic core and stretched alkyl chains (see Fig. 2f and g and Table 2). This indicates a monolayer structure; in the layers the packing should preferably be antiparallel due to the steric dipole[81] provided by the distinct cross sectional areas of the bulky 3,7-dimethyloctyloxy group at one end and the slim *n*-alkyl chain at the other end. In this arrangement the effective layer distance can be affected by the degree of interdigitation and intercalation of the molecules. There are at least two distinct modes of this antiparallel packing, shown in Fig. 2f and g. One with optimized core packing density does not allow a complete segregation of the aromatic and aliphatic units (Fig. 2f). The alternative organization allows the densest packing of the aliphatic chains and full core-chain segregation, but it also leads to some distortion of the packing of the bent cores, due to the different lengths of the two wings at the central 1,3-substituted benzene ring (Fig. 2g). In this packing mode the effective layer distance would be 5.4 nm, which exceeds the molecular length. This difference between expected and measured layer thickness in the SmA phases is in line with the proposed tilted organization of the molecules in tilt-randomized domains (with β up to 19°).

Compound *rac*-**10**, as a representative example showing the complete series of different LC phases ranging from SmA to Col_{obl}, was investigated by XRD in the temperature range of the four different smectic phases (Fig. 7a). Already a few degrees

Table 2 Lattice parameters of the investigated columnar phases, molecular lengths, estimated optical tilt angles and temperatures of inversion of birefringence (T_{inv})[a]

Compd.	T/°C	Phase	a/nm	b/nm	γ/°	d_{diff}	L_{mol}/nm	β/°	T_{inv}/°C
rac-**6**	140	Col_{obl}	7.1	4.5	104	0.46	5.2	~8	—
rac-**8**	145	Col_{obl}	7.6	4.6	98	0.47	5.4	~12	—
rac-**10**	120	(pseudo) Col_{rec}	8.5	5.0	(90)	0.44	5.6	~14	—
rac-**11**	120	(pseudo) Col_{rec}	9.6	4.8	(90)	0.46	5.7	~16	138
(*S*)-**11**	120	(pseudo) Col_{rec}	7.7	5.0	(90)	0.47	5.7	~14	139
rac-**12**	—	—	—	—	—	—	5.8	~18	130
(*S*)-**12**	—	—	—	—	—	—	5.8	~15	130
rac-**14**	120	Col_{obl}	8.1	5.1	98	0.48	6.0	~20	115

[a] d_{diff} = maximum of the diffuse wide angle scattering, L_{mol} was determined for the conformation shown in Fig. 2f and g, β is the optical tilt in the Col phases.

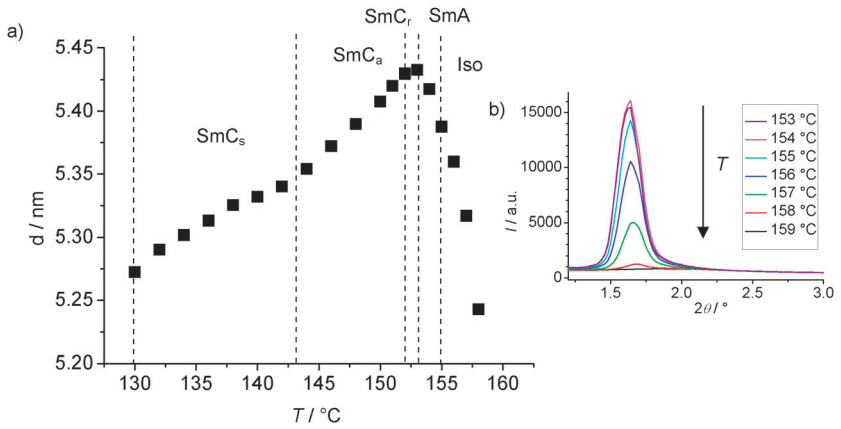

Fig. 7 XRD investigation of compound *rac*-**10**: (a) temperature dependence of the *d*-value of the layer reflection in the temperature range of the smectic phases and (b) the change of the profile of the small angle scattering depending on temperature in the temperature range of the Iso and SmA phases.

above the SmA–Iso transition, at T = 158 °C, a cybotactic character of the isotropic liquid phase can be observed by the significant growth of the intensity of the diffuse small angle scattering until the Iso–SmA transition is reached at T = 154 °C (Fig. 7b). In the smectic phases and the columnar phase a diffuse wide angle scattering around d = 0.47 nm confirms fluid LC phases without in-plane order (Table S1 and Fig. S8a and b, ESI†). The increased lateral mean distance compared with the usually observed value of 0.45 nm should be mainly due to the bulky double branched 3,7-dimethyloctyloxy chains, giving rise to an increased mean lateral distance between the molecules. Below T = 154 °C there is a sharp small angle scattering without detectable second order reflection, confirming lamellar phases with d values between d = 5.27 and d = 5.43 nm for all LC phases of compound *rac*-**10**, depending on temperature and phase type. The absence of any higher order reflection indicates rather diffuse interlayer interfaces. The d-value in the SmA phase corresponds to 0.94–0.97 of the single molecular length L_{mol} = 5.6 nm. This allows a slightly tilted organization with a maximum molecular tilt of 14–20°. In the temperature range of the SmA phase the d-value increases from d = 5.38 nm at the Iso–SmA transition to the maximum of d = 5.43 nm at T = 153 °C when the transition to the SmC$_r$ phase takes place. This increase in the d-value can be explained by chain stretching due to a growing packing density of the molecules with decreasing temperature. At T = 153 °C the increase of d stops at the transition to the SmC$_r$ phase and in the SmC$_r$, SmC$_a$ and SmC$_s$ phase ranges a decrease of the d-value is observed, in line with a further increasing tilt (Fig. 7a).

For all investigated compounds the layer distances in the various smectic phases are in the same range (approximately between 5.0 and 5.4 nm) and there is no clear relation between alkyl chain length and d-values (see Table S1, ESI†). This is in line with growing conformational disorder and increasing tilt with the increasing chain length and possibly is also affected by a chain length dependent contribution of the distinct packing modes shown in Fig. 2f and g. The tilt is small in all smectic and columnar phases, typically in the range between 8 and 20°, as estimated from planar textures (see Table 2 and Fig. 5).[82]

2.4 XRD investigation of the columnar phases

The columnar phases of compounds *rac*-**6** (Fig. 6b), *rac*-**10** (Fig. S8d, ESI†), *rac*-**11** (Fig. 8a) and *rac*-**14** (Fig. 8b) were investigated by 2D SAXS of surface aligned samples (Table 2 and Table S1, ESI†). The columnar phase of *rac*-**6** shows an oblique lattice ($p2$) with parameters a = 7.1 nm, b = 4.5 nm and γ = 104° (see Fig. 6b). This confirms a synclinic tilted ribbon structure of this columnar phase with parameter a corresponding to the lateral diameter of the ribbons and b approximately corresponding to the thickness of the ribbons as determined by the molecular length (L_{mol} = 5.2 nm) and the tilt of the molecules with respect to the a-axis of the oblique lattice.

The diffraction patterns of *rac*-**10** and *rac*-**11** were indexed to non-centred rectangular lattices with plane group $p2mm$ and parameters a = 8.5 nm, b = 5.0 nm for *rac*-**10** and a = 9.6 nm, b = 4.8 nm for *rac*-**11** (see Fig. 8a and Fig. S8, and Table 2 and

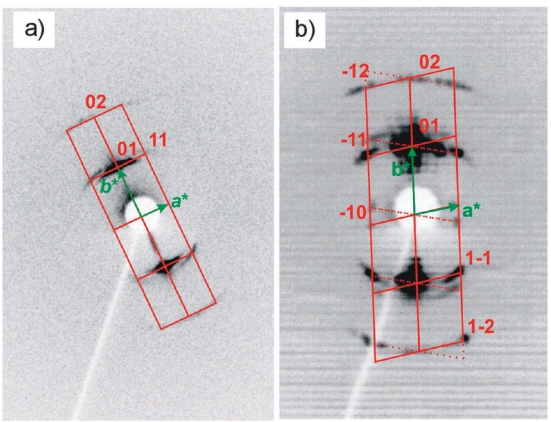

Fig. 8 (a, b) 2D XRD patterns of the columnar phases: (a) Col$_{rec}$ phase of *rac*-**11** at T = 110 °C with indexation to a rectangular $p2mm$ lattice with a = 9.57 nm, b = 4.80 nm; (b) Col$_{obl}$ phase of *rac*-**14** at T = 120 °C with indexation to an oblique $p2$ lattice with a = 8.06 nm, b = 5.12 nm and γ = 98.3°.

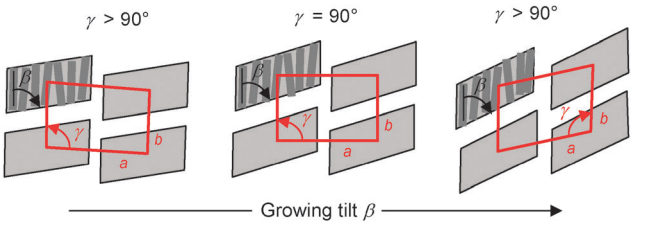

Fig. 9 Changing of the tilt β of the molecules in the ribbons and retaining the degree of longitudinal shift of the ribbons leads to a change in the oblique angle γ with crossing of the 90° angle; it has to be considered that the larger angle is always chosen as γ.

Table S1, ESI†). Interestingly *rac*-**14** has again an oblique lattice with a = 8.1 nm, b = 5.1 nm and γ = 98° (Fig. 8b). Though rectangular and oblique lattices were observed, in all columnar phases the extinctions in the textures of highly birefringent planar aligned samples are inclined with the directions of the polarizers, indicating a synclinic tilt (see inset in Fig. 3e and Fig. S2d, and Fig. 2c and 5 and Fig. S3c, ESI†). The tilt increases with growing chain length from $\beta \sim 8°$ for *rac*-**6** *via* $\beta \sim 12°$ for *rac*-**8** and $\beta \sim$ 14–18° for *rac*-**10**–*rac*-**12** to $\beta \sim 20°$ for *rac*-**14** (see Table 2). Therefore, it is suggested that all columnar phases represent oblique phases with changing oblique angle going through $\gamma \sim 90°$ for the case of the pseudo-rectangular lattices observed for *rac*-**10** and *rac*-**11** with intermediate chain length. As shown in Fig. 9 this can easily be achieved by increasing the tilt angle of the molecules in the ribbons.

2.5 Inversion of birefringence in the columnar phases

Whereas in planar aligned samples of the Col_{obl}/Col_{rec} phases (high birefringent textures, see Fig. 2c, 3e and 5 and Fig. S2d and S3c, ESI†) the extinction crosses are inclined with the directions of the polarizers, indicating the tilt of the molecules, in homeotropic samples (low birefringent textures, see Fig. 2d and 3f and Fig. S1d, ESI†) the extinction crosses are always parallel to the polarizers. In this homeotropic alignment of the ribbons (with the ribbon normal perpendicular to the substrate surfaces) the direction of birefringence provides additional information about molecular self-assembly. In homeotropic alignment the columnar phases of *rac*-**6** to *rac*-**10** are optically positive as deduced from investigation with a λ-retarder plate, shown in Fig. 2e for *rac*-**6** and in Fig. 3f for *rac*-**8** (for *rac*-**10**, see inset in Fig. S1d, ESI†). This means that the slow optical axis, which is along the longest intramolecular π-conjugation path, is parallel to the ribbon long axis, *i.e.* either the tilt or the main direction of molecular biaxiality is along the ribbon long axis (Fig. 10e and f). Though XRD and optical investigation of planar samples confirmed tilt in the *a*–*b* plane of the 2D lattice, it cannot be excluded that an additional tilt along the *c* direction ("leaning" along the ribbon long axis) would be possible, as known for the SmC_G phases.[15,16] Because in homeotropic alignment the extinction crosses are parallel to the polarizers (Fig. 2d and 3f) a synclinic leaning can be excluded. Based on optical observations an antileaning SmC_G phase could in principle be possible, but there is no XRD evidence (double layer structure)

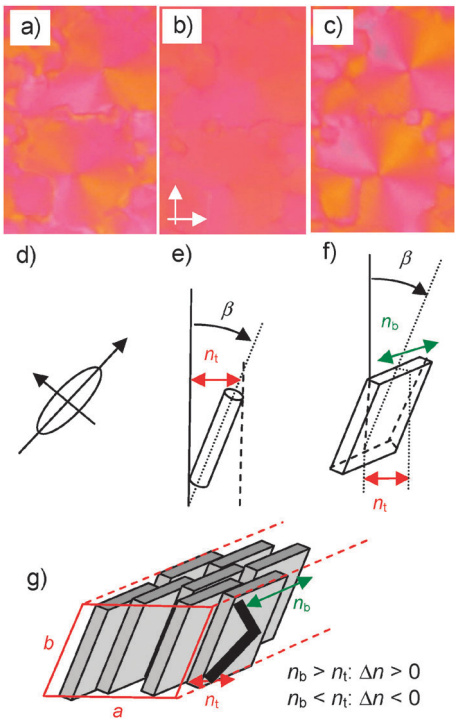

Fig. 10 Inversion of the birefringence in the columnar phase region of compound (*S*)-**12** as observed between crossed polarizers (orientation indicated by arrows in (b) with an additional λ-retarder plate; indicatrix orientation is shown in (d)); (a) immediately after the SmC_s–Col phase transition at T = 135 °C the birefringence is negative (direction of the blue shifted segments of the spherulites is north east and south west), (b) close to the inversion point at T = 129 °C it is about zero (spherulites are nearly invisible) and (c) at T = 112 °C it is positive (direction of the blue shifted segments of the spherulites is north west and south east); (d) shows the indicatrix orientation and (e, f) illustrate the contributions (e) of tilt (n_t) and (f) restricted molecular rotation (n_b) to birefringence; (g) shows a model for the organization of compounds *rac*-***n*** in the Col_{obl} phases with $Col_{rev.tilt}$ like structure.

for such a phase.[16] As a SmC_G structure is discarded, the positive birefringence of the columnar phases of compounds *rac*-***n*** with n = 6–10 should be due to the dominance of the molecular biaxiality (n_b), resulting from the reduced rotational disorder around the molecular long axis. In this case the molecular biaxiality n_b, which is normal to the tilt direction and parallel to the ribbon long axis, has to be larger than the biaxiality caused by the tilt (n_t), *i.e.* $n_b > n_t$ (see Fig. 10f). The dominance of molecular biaxiality indicates a dense packing and restricted rotation of the bent aromatic cores in the ribbons of these Col_{obl}/Col_{rec} phases. It also confirms an alignment of the bend-planes parallel to the ribbon long axis and that the tilt direction is perpendicular to this axis as typical for $B1_{rev,tilt}$ phases (Fig. 10g).[83]

Interestingly, for compounds *rac*-**12** and *rac*-**14** an inversion of the direction of the birefringence is observed in the columnar phase range (Fig. 10a–c). For *rac*-**12** (and (*S*)-**12**) the birefringence is negative immediately after the phase transition SmC_s–Col, goes through $\Delta n = 0$ at $T \sim 130$ °C and becomes positive below this temperature. Moreover, there is a chain length dependence

of the inversion point (see Table 2). With growing alkyl chain length the inversion point is shifted to lower temperatures; for *rac*-**12** it is at $T \sim 130$ °C and decreases further to $T \sim 115$ °C for compound *rac*-**14** with the longest alkyl chain. For *rac*-**11** (and (*S*)-**11**) with a bit shorter chain the inversion point coincides with the SmC_s–Col_{rec} transition at $T \sim 138$ °C. Thus, in the Col_{rec} phase of *rac*-**12** (and (*S*)-**12**) the birefringence is positive, as found for the columnar phases of the shorter homologues *with* $n = 6$–10. This chain length dependent change of the direction of the slow optical axis from being parallel to the ribbon long axis to perpendicular can be explained by the increasing tilt with growing alkyl chain length (Table 2), leading to an increasing contribution of n_t. With decreasing temperature there is a transition from negative back to positive birefringence, which is neither associated with any peak in the DSC traces nor by a change of the XRD pattern. This can be explained by the growing packing density at lower temperature. Thus, the rotation of the molecules around their long axes becomes increasingly restricted which increases the contribution of the molecular biaxiality n_b to the overall birefringence. The temperature dependence of n_b appears to be larger than the temperature dependent change of n_t and thus the birefringence becomes positive again below a certain critical temperature (see Fig. 10e–g).

For compounds *rac*-**12**, (*S*)-**12** and *rac*-**14** the birefringence does not change at the phase transitions Col–SmC_s–SmC_a so it is assumed that also in the smectic phases of these compounds the tilt determines the direction of the slow axis and with increasing chain length its influence becomes increasingly dominating. Probably for this reason, the typical stripe pattern disappears nearly completely for the SmC_a phase of *rac*-**14** with the longest chain (see Fig. S3d, ESI†). For compound *rac*-**11**, (*S*)-**11** Δn is inverted at the Col–SmC_s phase transition, whereas for compounds *rac*-**6** to *rac*-**10** no inversion of the birefringence could be observed. Therefore, it is assumed that in the SmC phases of compounds *rac*-**10**, *rac*-**11** and (*S*)-**11** the direction of the slow axis should also be determined by the molecular biaxiality as in the columnar phases. For *rac*-**8** with the smallest tilt it could be speculated that there is nearly no molecular biaxiality or the directions of tilt and the secondary director coincide, leading to a distinct appearance (*e.g.* missing stripe pattern in homeotropic alignment) of the SmC phase of this compound, similar to usual SmC phases as known from rod-like LC.

2.6 Electro-optic investigations

In the temperature range of the smectic and columnar phases of all compounds *rac*-***n*** with $n = 4$–14 there is no current response observed under a triangular wave field up to the maximum available value of 60 V μm^{-1} (peak-to-peak) indicating the absence of polar switching. Also optical investigations confirm the absence of polar switching. This means that either polar order is absent or it has only a short coherence length. We mainly attribute this to the bulkiness of the branched 3,7-dimethyloctyloxy groups which reduce the lateral packing density, as indicated by the shift of the maximum of the diffuse wide angle scattering maximum from the typical value $d = 0.44$–0.45 nm to larger values around $d = 0.47$ nm for the smectic phases of compounds *rac*-***n*** (see Table 2 and Table S1, ESI†). This apparently disfavours the polar packing of the bent core units. The bulkiness of the 3,7-dimethyloctyloxy groups appear to be also mainly responsible for a steric layer frustration leading to development of layer modulation at the transition to the columnar phases. In these columnar phases the lateral interfaces between the ribbons are known to suppress polar switching,[2] even if there would be polar order along the ribbons.

2.7 Chirality effects

In order to study the effects of the molecular chirality on the mesophases the enantiomers (*S*)-**11** and (*S*)-**12** were synthesised and investigated. They exhibit the same LC phases with almost the same transition temperatures as the racemic mixtures *rac*-**11** and *rac*-**12**, respectively (see Table 1). The birefringence of the homeotropic schlieren texture of the SmC_s* phases is much lower compared to the SmC_s phases of the racemates (see Fig. S2, ESI†), in line with the presence of a helical superstructure parallel to the layer normal having a pitch length significantly longer than the wavelength of visible light. The presence of a helical superstructure is also evident from the finger print textures in the planar samples of the SmC_s* phases, where, in addition, a distinct color shift was observed upon uncrossing the polarizers by a small angle in the (−) or (+) direction (see Fig. S4b, c, e–g and S5b, ESI†). At an angle of about 35° between the directions of the polarizers (6 μm cells) dark extinctions can be observed (see inset in Fig. S4c, ESI†), suggesting a helical pitch length exceeding the cell gap. The birefringence of the homeotropic aligned SmC_a* phase of the enantiomers compared to the racemates is not reduced to that extend as found for the SmC_s* phase (Fig. S2 a–g, ESI†) and in most cases there is no fingerprint texture in the planar samples of the SmC_a* phases, in line with a much reduced helical twist due to the weaker layer coupling in these anticlinic LC phases (see Fig. S4a and S5a, ESI†).

There is no clear indication of polar switching in any of the smectic phases of (*S*)-**11**. Only for compound (*S*)-**12** in the temperature range of the anticlinic SmC_a* phase, assigned as the SmC_aP_R* phase, a single peak is observed in the switching current curves, in line with a ferroelectric switching with $P_S = 330$ nC cm^{-2} (Fig. 11). This single peak is reproducibly observed in non-coated as well as in PI coated ITO cells (see Fig. S14, ESI†) and disappears in both cases at the transition to the isotropic liquid and to the SmC_s* phase. The disappearence of the peak at both phase transitions confirms that it is not due to conductivity, and the fact that switching is only observed for the enantiomer and not for the racemic mixture indicates that chirality is essential for this switching process. In this respect (*S*)-**12** behaves like a chiral rod-like molecule. However, in anticlinic tilted SmC_A* phases of rod-like mesogens an antiferroelectric switching process with two peaks in each half period of the triangular wave field (by rotation on a cone) would be expected to take place instead of a ferroelectric one, indicated by the single peak. So, the bent molecular shape

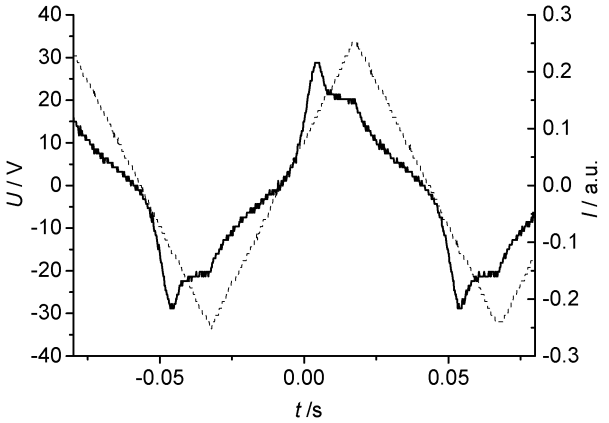

Fig. 11 (a) Switching current response obtained for (*S*)-**12** in the SmC_aP_R* phase under a triangular wave field (T = 150 °C, U = 66 V_{pp}, f = 10 Hz, 5 μm non-coated ITO cell, P_S = 330 nC cm^{-2}).

should be of major importance and appears to determine the switching mode. This kind of relatively broad peak was previously observed for randomized polar phases ($SmAP_R$[33,34] and $SmCP_R$ phases[84]) where ferroelectric domains with an appreciable size, growing under the applied field, were switched. Thus it could be hypothesized that the switching is $SmCP_R$-like and the development of polar order, leading to an increased polar domain size in the SmC_aP_R* phase, is supported by the applied electric field and the chiral recognition in the layers.[85] This means that the switching process is mainly based on the polar order of the bent cores. Also the relatively high polarization value is in line with a bent-core based switching process for this kind of molecules, with a stereogenic centre in the terminal alkyl chain being only weakly coupled with the aromatic core. The fact that polar switching is absent in the SmC_s* phase at lower temperature is surprising and could have different reasons. It might be due to an increased viscosity, the presence of a helical superstructure which is not sufficiently unwinded, or due to the emergence of some layer modulations occuring already in the temperature range of the SmC_s* phase.

At the transition to the columnar phases the helical superstructure is completely removed as indicated by the removal of the finger print texture, the completely dark extinction crosses in the fan-like mosaic textures of the planar aligned Col phases (see Fig. S4c, d and h, ESI†) and the absence of an effect of the direction of uncrossing of the polarizers on the colour of the texture.[86] As already found for the racemates, none of the columnar phases shows any switching current peak. XRD investigation of the columnar phase of the enantiomer (*S*)-**11** indicates a pseudo-rectangular lattice, as also found for the racemic mixture *rac*-**11**. The lattice parameter a = 7.7 nm (corresponding to the width of the ribbons) is nearly two nanometer smaller than that found for the racemic compound whereas the thickness of the ribbons b = 5.0 nm is only marginally larger (see Table 2 and Table S1, ESI†). The different a-parameter could be due to a slightly distinct packing density of homogeneously chiral molecules compared to the racemic mixture. Indeed, the diffuse wide angle XRD maximum is shifted from 0.46 nm (*rac*-**11**) to 0.48 nm for (*S*)-**11**, in line with a reduced packing density in the Col_{rec} phase of (*S*)-**11**. The reduced packing density leads to a stronger steric layer frustration and thus to ribbons with a smaller width for (*S*)-**11**.

3. Summary and conclusions

A new series of unsymmetrical 6-ring bent-core compounds derived from 4′-hydroxybiphenyl-3-carboxylic acid with a bulky 3,7-dimethyloctyloxy group at one end has been synthesized. The LC phases appear to be dominated by the competition between dense polar packing of the bent aromatic cores and their separation by the bulky 3,7-dimethyloctyloxy groups. Thus, five types of smectic phases (SmA, SmC, SmC_r, SmC_a, SmC_s) and a columnar phase, either with oblique (Col_{obl}) or pseudo-rectangular lattice (Col_{rec}), were observed. The lower homologues show a special type of uniaxial SmA phase for which a lamellar organization of the sub-micrometer sized SmC domain with small tilt and randomized tilt direction is proposed. On increasing the number of carbon atoms in the terminal alkoxy chain this de Vries-like uniaxial SmA phase is stepwise replaced by a series of biaxial LC phases. An ordinary SmC phase is only found for *rac*-**8**. For the compound with a slightly longer n-alkyl chain (n = 10) an unusual LC phase is observed, where weakly tilted SmC_s domains obviously reach an appreciable size allowing the coupling of the tilt direction under the influence of surface stabilization. At reduced temperature or by further increasing the chain length ($n \geq 11$) this intermediate SmC_r phase is replaced by a SmC_a phase, also having a relatively small tilt, thus providing only weak tilt coupling between adjacent layers. The weak layer correlation leads to SmC_s layer stacks with a high density of anticlinic layers between them, overall appearing like an anticlinic SmC_a phase. Further reducing the temperature raises the tilt further and thus reinforces the layer coupling, favouring synclinic tilt correlation and leading to a nearly continuous transition to the SmC_s phase without anticlinic defects. As the tilt is associated with a denser packing of the bent aromatic cores it enhances the barrier for the rotation around the molecular long axis, providing molecular biaxiality. The increased packing density also gives rise to the emergence of layer modulations, contributing to the removal of anticlinic defects in the SmC_s phase, and adopting a long range correlation at the transition to the columnar phases. In all Col phases the tilt is synclinic and with a growing alkyl chain length there is a transition from Col_{obl} *via* a pseudo-rectangular columnar phase with an oblique angle $\gamma = 90°$ (Col_{rec}) to Col_{obl} again, which is explained by the continuous increase of the tilt angle with rising chain length. In the Col phases the organization is $B1_{rev}$-like, *i.e.* the molecular rotation around the long axis is restricted with the bend-planes aligned parallel to the long column axis and the tilt being perpendicular to the columns. The orthogonal combination of tilt and molecular biaxiality leads to a competition between them. For the columnar phases of compounds with short chains, having only a small tilt, the molecular biaxiality is

dominating, and hence, birefringence is positive. With the rising chain length the tilt rises and becomes dominating and hence the biaxiality becomes negative. However, at reduced temperature, as rotation around the long axis becomes increasingly restricted, the molecular biaxiality becomes dominating again. Besides long range correlation of molecular biaxiality there might also be local polar correlation between the molecules, but the coherence length of polar order appears to be too short to provide polar switching. Ferroelectric-like switching is induced by molecular chirality in the SmC_a* phase region (SmC_aP_R*) of one of the (*S*)-enantiomers. Here the local polar order of the bent aromatic cores within the layers seems to be supported by chiral recognition.

Overall, the length of the linear alkyl chain influences the mode of self-assembly by increasing the attractive intermolecular dispersion forces with growing chain length, leading to increased packing density. The increased packing density provides a tilt and restricted molecular rotation, which then affect the degree of layer coupling and steric frustration, thus leading to feedback and development of complex regulatory networks determining the mode of molecular self assembly in the resulting LC phases. Hence, this series of compounds provides an interesting showcase for the complex relations involved in the combined development of polar order,[5,40] domain size, tilt, tilt correlation and layer modulation in fluid self assembled systems, depending on the molecular structural information. Thus, this work provides basic knowledge on the further optimization of bent-core based LC materials aiming at the directed design of specific phase structures for use in future applications.

4. Experimental

The synthesis of the final compounds and intermediates (Scheme 1), and analytical data are reported in detail in the ESI.† Purification was performed by column chromatography (silica gel 60, Merck, pore size 60 Å, 230–400 mesh) followed by crystallization using the solvents described in the ESI.† ^{1}H- and ^{13}C-NMR were recorded using Varian Unity 500 and Varian Unity 400 spectrometers in $CDCl_3$ solutions with tetramethylsilane as the internal standard. MS were recorded with an AMD 402 (electron impact, 70 eV). Microanalyses were performed using a Leco CHNS-932 elemental analyzer.

Transition temperatures were measured and optical investigations were carried out using a Mettler FP-82 HT hot stage and a control unit in conjunction with a Leica Leitz DMR polarizing microscope. Transition temperature measurement and optical inspection of the liquid crystalline phases were performed on samples between ordinary glass slides. The associated enthalpies were obtained from DSC-thermograms which were recorded on a Perkin-Elmer DSC-7 in 30 μl-pans for 3–5 mg samples with heating and cooling rates of 10 K min^{-1}; peak temperatures from the first heating and cooling scans are given in Table 1. X-ray diffraction patterns of aligned samples were recorded using a 2D detector (HI-STAR, Siemens or Vantec 500, Bruker). Ni filtered and pin hole collimated Cu-K_α radiation was used. Alignment was achieved by slow cooling (0.1 K min^{-1}) of a small droplet on a glass surface; the beam was applied parallel to the surface. Powder samples were taken in thin capillaries ($\varnothing$ = 1 mm). The sample to detector distance was 8.8 cm and 26.9 cm for the wide angle and small angle measurements, respectively, and the exposure time was 60 min. Switching experiments and electro-optical investigations were performed in 5 μm non-coated and 6 μm polyimide (PI) coated ITO cells (EHC, Japan) with a measuring area of 1 cm^2 (antiparallel rubbing in the PI-coated cells). The cells were filled at the isotropic state. Switching experiments were carried out with the triangular wave method[87] using a combination of a function synthesizer (Agilent, model 33220A), amplifier (FLC electronics, model A400), and the current response traces were recorded using an oscilloscope (Tektronix, model TDS2014) across a 5 kΩ resistance.

Acknowledgements

H. O. is grateful to the Alexander von Humboldt Foundation and the Joachim Herz Stiftung for a research fellowship at Martin Luther University, Halle, Germany; B. B.-E. is grateful to the Alexander von Humboldt Foundation for financial support toward liquid crystal research; and M.P. and C.T. acknowledge the support from the DFG (Ts 39/24-1).

References

1 H. Takezoe and Y. Takanishi, *Jpn. J. Appl. Phys.*, 2006, **45**, 597–625.
2 R. A. Reddy and C. Tschierske, *J. Mater. Chem.*, 2006, **16**, 907–961.
3 D. M. Walba, E. Körblova, R. Shao, J. E. Maclennan, D. R. Link, M. A. Glaser and N. A. Clark, *Science*, 2000, **288**, 2181–2184.
4 J. Etxebarria and M. B. Ros, *J. Mater. Chem.*, 2008, **18**, 2919–2926.
5 A. Eremin and A. Jakli, *Soft Matter*, 2013, **9**, 615–637.
6 G. Pelzl, A. Eremin, S. Diele, H. Kresse and W. Weissflog, *J. Mater. Chem.*, 2002, **12**, 2591–2593.
7 H. Nadasi, W. Weissflog, A. Eremin, G. Pelzl, S. Diele, B. Das and S. Grande, *J. Mater. Chem.*, 2002, **12**, 1316–1324.
8 J. P. F. Lagerwall and G. Scalia, *Curr. Appl. Phys.*, 2012, **12**, 1387–1412.
9 H. Kim, Y. H. Kim, S. Lee, D. M. Walba, N. A. Clark, S. B. Lee and D. K. Yoona, *Liq. Cryst.*, 2014, **41**, 328–341.
10 W. Iglesias and A. Jakli, in *Handbook of Liquid Crystals*, ed. J. W. Goodby, P. J. Collings, T. Kato, C. Tschierske, H. F. Gleeson and P. Raynes, Wiley-VCH, Weinheim, 2nd edn 2014, vol. 8, pp. 799–814.
11 T. Niori, T. Sekine, J. Watanabe, T. Furukawa and H. Takezoe, *J. Mater. Chem.*, 1996, **6**, 1231–1233.
12 D. Shen, A. Pegenau, S. Diele, I. Wirth and C. Tschierske, *J. Am. Chem. Soc.*, 2000, **122**, 1593–1601.

13 J. Mieczkowski, J. Szydlowska, J. Matraszek, D. Pociecha, E. Gorecka, B. Donnio and D. Guillon, *J. Mater. Chem.*, 2002, **12**, 3392–3399.
14 V. Prasad, *Liq. Cryst.*, 2001, **28**, 145–150.
15 N. Chattham, E. Korblova, R. Shao, D. M. Walba, J. E. Maclennan and N. A. Clark, *Liq. Cryst.*, 2009, **36**, 1309–1317.
16 A. Kovářová, S. Světlík, V. Kozmík, J. Svoboda, V. Novotná, D. Pociecha, E. Gorecka and N. Podoliak, *Beilstein J. Org. Chem.*, 2014, **10**, 794–807.
17 D. A. Coleman, J. Fernsler, N. Chattham, M. Nakata, Y. Takanishi, E. Körblova, D. R. Link, R.-F. Shao, W. G. Jang, J. E. Maclennan, O. Mondainn-Monval, C. Boyer, W. Weissflog, G. Pelzl, L.-C. Chien, J. Zasadzinski, J. Watanabe, D. M. Walba, H. Takezoe and N. A. Clark, *Science*, 2003, **301**, 1204–1211.
18 S. Radhika, H. T. Srinivasa and B. K. Sadashiva, *Liq. Cryst.*, 2011, **38**, 785–792.
19 P. Sathyanarayana, S. Radhika, B. K. Sadashiva and S. Dhara, *Soft Matter*, 2012, **8**, 2322–2327.
20 H. Ocak, B. Bilgin-Eran, M. Prehm, S. Schymura, J. P. F. Lagerwall and C. Tschierske, *Soft Matter*, 2011, **7**, 8266–8280.
21 G. Pelzl and W. Weissflog, in *Thermotropic Liquid Crystals: Recent Advances*, ed. A. Ramamoorthy, Springer, Berlin, 2007, pp. 1–58.
22 C. Keith, A. Lehmann, U. Baumeister, M. Prehm and C. Tschierske, *Soft Matter*, 2010, **6**, 1704–1721.
23 G. Shanker, M. Prehm, M. Nagaraj, J. K. Vij, M. Weyland, A. Eremin and C. Tschierske, *ChemPhysChem*, 2014, **15**, 1323–1335.
24 O. Francescangeli, F. Vita and E. T. Samulski, *Soft Matter*, 2014, **10**, 7685–7691.
25 B. K. Sadashiva, R. A. Reddy, R. Pratibha and N. V. Madhusudana, *Chem. Commun.*, 2001, 2140–2141.
26 B. K. Sadashiva, R. A. Reddy, R. Pratibha and N. V. Madhusudana, *J. Mater. Chem.*, 2002, **12**, 943–950.
27 R. A. Reddy and B. K. Sadashiva, *J. Mater. Chem.*, 2004, **14**, 310–319.
28 C. V. Yelamaggad, I. S. Shashikala, D. S. S. Rao, G. G. Nair and S. K. Prasad, *J. Mater. Chem.*, 2006, **16**, 4099–4102.
29 C. V. Yelamaggad, I. S. Shashikala, V. P. Tamilenthi, D. S. S. Rao, G. G. Nair and S. K. Prasad, *J. Mater. Chem.*, 2008, **18**, 2096–2103.
30 K. J. K. Semmler, T. J. Dingemans and E. T. Samulski, *Liq. Cryst.*, 1998, **24**, 799–803.
31 R. Pratibha, N. V. Madhusudana and B. K. Sadashiva, *Mol. Cryst. Liq. Cryst.*, 2001, **365**, 755–776.
32 R. Pratibha, N. V. Madhusudana and B. K. Sadashiva, *Science*, 2000, **288**, 2184–2187.
33 (*a*) D. Pociecha, M. Cepic, E. Gorecka and J. Mieczkowski, *Phys. Rev. Lett.*, 2003, **91**, 185501; (*b*) Y. Shimbo, E. Gorecka, D. Pociecha, F. Araoka, M. Goto, Y. Tankanishi, K. Ishikawa, J. Mieczkowski, K. Gomola and H. Takezoe, *Phys. Rev. Lett.*, 2006, **97**, 113901.
34 C. Keith, M. Prehm, Y. P. Panarin, J. K. Vij and C. Tschierske, *Chem. Commun.*, 2010, **46**, 3702–3704.
35 M. Gupta, S. Datta, S. Radhika, B. K. Sadashiva and A. Roy, *Soft Matter*, 2011, **7**, 4735–4741.
36 B. K. Sadashiva, V. A. Raghunathan and R. Pratibha, *Ferroelectrics*, 2000, **243**, 249–260.
37 A. Eremin, S. Diele, G. Pelzl, H. Nadasi, W. Weissflog, J. Salfetnikova and H. Kresse, *Phys. Rev. E: Stat., Nonlinear, Soft Matter Phys.*, 2001, **64**, 051707.
38 R. A. Reddy, C. Zhu, R. Shao, E. Korblova, T. Gong, Y. Shen, E. Garcia, M. A. Glaser, J. E. Maclennan, D. M. Walba and N. A. Clark, *Science*, 2011, **332**, 72–77.
39 U. Dunemann, M. W. Schroder, R. A. Reddy, G. Pelzl, S. Diele and W. Weissflog, *J. Mater. Chem.*, 2005, **15**, 4051–4061.
40 D. Pociecha, E. Gorecka, M. Cepic, N. Vaupotic and W. Weissflog, *Phys. Rev. E: Stat., Nonlinear, Soft Matter Phys.*, 2006, **74**, 021702.
41 H. N. Shreeninvasa Murthy and B. K. Sadashiva, *Liq. Cryst.*, 2004, **31**, 567–578.
42 L. Guo, S. Dhara, B. K. Sadashiva, S. Radhika, R. Pratibha, Y. Shimbo, F. Araoka, K. Ishikawa and H. Takezoe, *Phys. Rev. E: Stat., Nonlinear, Soft Matter Phys.*, 2010, **81**, 011703.
43 Y. P. Panarin, M. Nagaraj, J. K. Vij, C. Keith and C. Tschierske, *EPL*, 2010, **92**, 26002.
44 M. Bremer, P. Kirsch, M. Klasen-Memmer and K. Tarumi, *Angew. Chem., Int. Ed.*, 2013, **52**, 8880.
45 M. Nagaraj, Y. P. Panarin, J. K. Vij, C. Keith and C. Tschierske, *Appl. Phys. Lett.*, 2010, **97**, 213505.
46 L. Kovalenko, M. W. Schröder, R. A. Reddy, S. Diele, G. Pelzl and W. Weissflog, *Liq. Cryst.*, 2005, **32**, 857–865.
47 S. Radhika, B. K. Sadashiva and R. Pratibha, *Liq. Cryst.*, 2010, **37**, 417–425.
48 The latter three cases require a small and polar cyano group at one of the terminal positions of the bent aromatic core for the formation of non-tilted smectic phases (SmA_b and $SmAP_F$) thus leading to smectic phases with double layer structure due to preferred antiparallel packing and partial intercalation.[47]
49 W. Weissflog, G. Naumann, B. Kosata, M. W. Schröder, A. Eremin, S. Diele, Z. Vakhovskaya, H. Kresse, R. Friedemann, S. Ananda Rama Krishnan and G. Pelzl, *J. Mater. Chem.*, 2005, **15**, 4328–4337.
50 S. A. R. Krishnan, W. Weissflog, G. Pelzl, S. Diele, H. Kresse, Z. Vakhovskaya and R. Friedemann, *Phys. Chem. Chem. Phys.*, 2006, **8**, 1170–1177.
51 W. Weissflog, H. N. S. Murthy, S. Diele and G. Pelzl, *Philos. Trans. R. Soc., A*, 2006, **364**, 2657–2679.
52 R. A. Reddy, U. Baumeister, J. L. Chao, H. Kresse and C. Tschierske, *Soft Matter*, 2010, **6**, 3883–3897.
53 M. Kohout, J. Svoboda, V. Novotna and D. Pociecha, *Liq. Cryst.*, 2011, **38**, 1099–1110.
54 (*a*) E. Chin, J. W. Goodby, J. S. Patel and J. M. Geary, *Mol. Cryst. Liq. Cryst.*, 1987, **146**, 325–339; (*b*) J. W. Goodby, E. Chin, J. M. Geary, J. S. Patel and P. L. Finn, *J. Chem. Soc., Faraday Trans. 1*, 1987, **83**, 3429–3446.
55 (*a*) N. Miyaura, T. Yanagi and A. Suzuki, *Synth. Commun.*, 1981, **11**, 513–519; (*b*) N. Miyaura and A. Suzuki, *Chem. Rev.*,

1995, **95**, 2457–2483; (*c*) M. Hird, G. W. Gray and K. J. Toyne, *Mol. Cryst. Liq. Cryst.*, 1991, **206**, 187–204.
56 C. Keith, R. A. Reddy, A. Hauser, U. Baumeister and C. Tschierske, *J. Am. Chem. Soc.*, 2006, **128**, 3051–3066.
57 P. C. Jocelyn and N. Polgar, *J. Chem. Soc.*, 1953, 132–137.
58 (*a*) H. Kondo, T. Okazaki, N. Endo, S. Mihashi, A. Yamaguchi, H. Tsuruta and S. Akutagawa, *Jpn. Kokai Tokkyo Koho*, JP 63033351 A 19880213, 1988; (*b*) E. Chin and J. W. Goodby, *Mol. Cryst. Liq. Cryst.*, 1986, **141**, 311–320.
59 S.-C. Kuo, K.-H. Lee, L.-J. Huang, L.-C. Chou, T.-S. Wu, T.-D. Way, J.-G. Chung, J.-S. Yang, C.-H. Huang and M.-T. Tsai, *PCT Int. Appl.*, WO 2012009519 A1 20120119, 2012.
60 C. V. Yelamaggad, U. S. Hiremath, S. A. Nagamani, D. S. S. Rao, S. K. Prasad, N. Iyi and T. Fujita, *Liq. Cryst.*, 2003, **30**, 681–690.
61 B. Otterholm, M. Nilsson, S. T. Lagerwall and K. Skarp, *Liq. Cryst.*, 1987, **2**, 757–769.
62 R. Achten, R. Cuypers, M. Giesbers, A. Koudijs, A. T. M. Marcelis and E. J. R. Sudhölter, *Liq. Cryst.*, 2004, **31**, 1167–1174.
63 R. Achten, A. Koudijs, M. Giesbers, A. T. M. Marcelis and E. J. R. Sudhölter, *Liq. Cryst.*, 2005, **32**, 277–285.
64 S. Balamurugan, P. Kannan, K. Yadupati and A. Roy, *Liq. Cryst.*, 2011, **38**, 1199–1207.
65 C. Tschierske and H. Zaschke, *J. Prakt. Chem.*, 1989, **331**, 365–366.
66 C. Keith, R. A. Reddy, M. Prehm, U. Baumeister, H. Kresse, J. L. Chao, H. Hahn, H. Lang and C. Tschierske, *Chem. – Eur. J.*, 2007, **13**, 2556–2577.
67 R. A. Reddy, U. Baumeister, C. Keith, H. Hahn, H. Lang and C. Tschierske, *Soft Matter*, 2007, **3**, 558–570.
68 G. S. Lee, Y.-J. Lee, S. Y. Choi, Y. S. Park and K. B. Yoon, *J. Am. Chem. Soc.*, 2000, **122**, 12151.
69 H. Ocak, B. Bilgin-Eran, M. Prehm and C. Tschierske, *Soft Matter*, 2012, **8**, 7773–7783.
70 H. Ocak, B. Bilgin-Eran, M. Prehm and C. Tschierske, *Soft Matter*, 2013, **9**, 4590–4597.
71 (*a*) A. De Vries, *J. Chem. Phys.*, 1979, **71**, 25–31; (*b*) S. T. Lagerwall, P. Rudquist and F. Giesselmann, *Mol. Cryst. Liq. Cryst.*, 2009, **510**, 148–157; (*c*) for a review see J. P. F. Lagerwall and F. Giesselmann, *ChemPhysChem*, 2006, **7**, 20–45.
72 These domains change their brightness by rotating the sample between crossed polarizers. However, the rotation of the analyzer by a small angle does not affect the relative brightness of the distinct domains; this indicates the absence of superstructural chirality.[1,2]
73 A sequence SmA–SmC_s–SmC_a was reported for hockey stick molecules: E. Enz, S. Findeisen-Tandel, R. Dabrowski, F. Giesselmann, W. Weissflog, U. Baumeister and J. Lagerwall, *J. Mater. Chem.*, 2009, **19**, 2950–2957.
74 T. Hegmann, J. Kain, S. Diele, G. Pelzl and C. Tschierske, *Angew. Chem., Int. Ed.*, 2001, **40**, 887–890.
75 R. Pratibha, N. V. Madhusudana and B. K. Sadashiva, *EPL*, 2007, **89**, 46001.
76 C. Y. Yelamaggad, I. S. Shashikala, V. P. Tamilenthi, D. S. S. Rao, G. G. Nair and S. K. Prasad, *J. Mater. Chem.*, 2008, **18**, 2096–2103.
77 A. Yoshizawa, M. Kurauchi, Y. Kohama, H. Dewa, K. Yamamoto, I. Nishiyama, T. Yamamoto, J. Yamamoto and H. Yokoyama, *Liq. Cryst.*, 2006, **33**, 611–619.
78 (*a*) Though not of relevance for the discussion herein, it should be mentioned that stripe patterns were also found for (a) the twist bent nematic phases of bent-core mesogens and (b) can be formed by elecroconvection patterns under an applied AC or DC electric field: V. P. Panov, R. Balachandran, J. K. Vij, M. G. Tamba, A. Kohlmeier and G. H. Mehl, *Appl. Phys. Lett.*, 2012, **101**, 234106; (*b*) D. Wiant, J. T. Gleeson, N. Eber, K. Fodor-Csorba, A. Jakli and T. Toth-Katona, *Phys. Rev. E: Stat., Nonlinear, Soft Matter Phys.*, 2005, **72**, 041712.
79 No information could be obtained for the enthalpy changes at the individual phase transitions SmA–SmC_r-SmC_a, as they are very close to each other and could possibly overlap. However, the total enthalpy change at these three transitions (4.4 kJ mol^{-1}) is close to the SmA–Iso transition enthalpy of the shorter homologue *rac*-**8** (4.7 kJ mol^{-1}), and therefore it is likely that the SmA–SmC_r and SmC_r-SmC_a transition enthalpies are small.
80 The texture of these SmC_s phases is very similar to the ''SmX-phases'' reported for hockey-stick molecules with the same 4′-hydroxybiphenyl-3-carboxylate based bent core unit, linear alkyl chains and reduced length of one of the legs, see ref. 18.
81 A. G. Petrov and A. Derzhanski, *Mol. Cryst. Liq. Cryst.*, 1987, **151**, 303–333.
82 The optical tilt mainly considers the tilt of the aromatic cores; the XRD tilt is usually significantly smaller and such small tilt angles cannot be determined directly with 2D XRD patterns from the orientation of the layer reflection with respect to the wide angle maximum as it is outside the precision of this method.
83 N. Vaupotic, D. Poiecha and E. Gorecka, *Top. Curr. Chem.*, 2012, **318**, 281–302.
84 (*a*) M. Alaasar, M. Prehm, M. Nagaraj, J. K. Vij and C. Tschierske, *Adv. Mater.*, 2013, **25**, 2186–2191; (*b*) M. Alaasar, M. Prehm, K. May, A. Eremin and C. Tschierske, *Adv. Funct. Mater.*, 2014, **24**, 1703–1717.
85 D. M. Walba, H. A. Razavi, A. Horiuchi, K. F. Eidman, B. Otterholm, R. C. Haltiwanger, N. A. Clark, R. Shao, D. S. Parmar, M. D. Wand and R. T. Vohra, *Ferroelectrics*, 1991, **113**, 21–36.
86 Already shortly before the transition to the Col phase the fingerprint texture is removed in the SmC_s* region, see Fig. S4c (ESI†).
87 K. Miyasato, S. Abe, H. Takezoe, A. Fukuda and E. Kuze, *Jpn. J. Appl. Phys.*, 1983, **22**, L661–L663.

